Understanding the origins of the intrinsic dead layer effect in nanocapacitors

M. S. Majdoub,[1] R. Maranganti,[1] and P. Sharma[1,2,*]
[1]*Department of Mechanical Engineering, University of Houston, Houston, Texas 77204, USA*
[2]*Department of Physics, University of Houston, Houston, Texas 77204, USA*
(Received 1 December 2008; revised manuscript received 26 January 2009; published 12 March 2009)

Thin films of high-permittivity dielectrics are considered ideal candidates for realizing high charge-density nanosized capacitors for use in next generation energy storage and nanoelectronic applications. The experimentally observed capacitance of such film nanocapacitors is, however, 1 order of magnitude lower than expected. This dramatic drop in capacitance is attributed to the so-called "dead layer"—a low-permittivity layer at the metal-dielectric interface in series with the high-permittivity dielectric. The exact nature of the dead layer and the reasons for its origin still remain somewhat unclear. Based on insights gained from recently published *ab initio* work on $SrRuO_3/SrTiO_3/SrRuO_3$ and our first-principles simulations on Au/MgO/Au and Pt/MgO/Pt nanocapacitors, we construct an analytical model that isolates the contributions of various physical mechanisms to the intrinsic dead layer. In particular we argue that strain-gradients automatically arise in very thin films even in absence of external strain inducers and, due to flexoelectric coupling, are dominant contributors to the dead layer effect. Our theoretical results compare well to existing as well as our own *ab initio* calculations and suggest that inclusion of flexoelectricity is necessary for qualitative reconciliation of atomistic results. Our results also hint at some remedies for mitigating the dead layer effect.

DOI: 10.1103/PhysRevB.79.115412 PACS number(s): 77.22.Ch, 77.90.+k, 85.35.−p

I. INTRODUCTION

Next generation advances in energy storage and nanoelectronics require capacitors fabricated at the nanoscale. High dielectric constant materials such as perovskite structures are important candidates for such applications. Consider the following: the expected capacitance (based on classical electrostatics) of a 2.7 nm $SrTiO_3$ (STO) thin film is $\sim$1600fF μm^{-2}. *Ab initio* simulations on $SrRuO_3/SrTiO_3/SrRuO_3$ (SRO/STO/SRO) capacitor system with the same dimensions however predict a much lower value—258fF μm^{-2}. This dramatic drop in capacitance is traditionally attributed to the so-called "dead layer" effect.[1] The dead layer is thought to be as a low-permittivity thin layer at the metal/dielectric interface connected in series with the rest of the dielectric. Indeed early experimental work by Mead and coworkers[2,3] and subsequently many others[4–7] documented the effects of the disruptive dead layer for nanometer sized films. The presence of this dead layer is attributed to a variety of reasons including a secondary low-permittivity phase at the surface of the films, nearby-surface variation of polarization (field induced or spontaneous),[8] presence of misfit dislocations,[9,10] and electric field penetration into the metal electrodes[11–14] among others. The effect of electric field penetration into the metal electrodes to explain the anomalous capacitance was proposed by Mead[2] himself and has since then been theoretically investigated by several authors.[11–14] Recent pioneering *ab initio* simulations by Stengel and Spaldin[15] on $SrRuO_3/SrTiO_3/SrRuO_3$ and $Pt/SrTiO_3/Pt$ thin-film capacitors with atomistically smooth interfaces (to exclude effects due to, say, misfit dislocations) confirmed the intrinsic nature of this effect and that electric field penetration does indeed occur in real metal electrodes giving rise to a passive dead layer at the metal-dielectric interface.

The effective capacitance C_{eff} of such a system with regions of low interfacial capacitance density at the metal-dielectric layer (i.e., the dead layer) C_i connected in series with the nominal capacitance C_0 of the dielectric is typically expressed as

$$\frac{1}{C_{\text{eff}}} = \frac{1}{C_i} + \frac{1}{C_0} + \frac{1}{C_i}. \tag{1}$$

The interfacial capacitance C_i is taken as the additional capacitance introduced into the system due to the penetration of the electric field into the metal electrodes, while the nominal capacitance C_0 of the dielectric layer is that predicted by classical electrostatics: for example, for a parallel-plate capacitor made up of a dielectric with dielectric permittivity ε and thickness d,

$$C_0 = \frac{\varepsilon}{d}. \tag{2}$$

The calculations performed by Stengel and Spaldin[15] provide a much deeper understanding of the origins of the dead layer. Indeed, their results, exemplified on the SRO/STO/SRO capacitor system, show that the physical picture painted by Eqs. (1) and (2) may be incorrect and certainly incomplete. In particular, their results show that the electrostatic potential profile in the dielectric part of the capacitor exhibits considerable nonlinear behavior (as opposed to the linear variation predicted by classical electrostatics) and that the capacitance of the dielectric layer C_0 is subject to some additional size-dependent scaling beyond what is suggested by Eq. (2) alone. We agree with the results of the *ab initio* work of Spaldin and Stengel,[15] however, in order to extract additional insights into the mechanism underpinning the dead layer, we construct a theoretical model of the possible underlying physical mechanisms and carry out *ab initio* calculations for other nanocapacitor systems. In this work, we argue that electric field penetration occurs inside the metal electrodes due to the diffuse nature of the metal-dielectric interface

 ©2009 The American Physical Society

which in turn triggers a secondary mechanism wherein intrinsic strain gradients arise in thin films activating the flexoelectric effect (strain gradient-induced polarization). Ironically, the *secondary* mechanism is found to dominate. Furthermore, our analytical approach allows a facile means to infer the correct scaling behavior of thin-film capacitance (something that is beyond the computational power of purely *ab initio* based simulations since the latter calculations are limited to a few nanometers thick films).

We note that the effect of strain gradients induced due to lattice mismatch in $Ba_{0.5}Sr_{0.5}TiO_3$ (BST) dielectric films grown on $SrRuO_3$ (SRO) metal electrodes was already investigated by Catalan *et al.*[16] who predicted that the large flexoelectric coefficients measured by Ma and Cross[17] and Zubko *et al.*[18] for ferroelectrics such as BST can potentially result in considerable changes in the polarization and permittivity behavior of thin-film ferroelectric capacitors. Since the *ab initio* simulations are performed in the absence of lattice mismatch effects. We shall ignore the presence of such *extrinsic* strains in the present work.

As mentioned previously, we postulate that the two dominant mechanisms responsible for polarization effects which lead to substantial decrease in the capacitance of thin dielectric-metal electrode capacitor systems are electric field penetration in metals and flexoelectricity in dielectrics, respectively. While the former is well evident from the *ab initio* results of Stengel and Spaldin,[15] the latter will be justified in due course by its ability to correctly (albeit qualitatively) predict the basics physics behind the dead layer. With appropriate information from *ab initio* results, quantitative agreement is also achieved. As will be shown in this work, failure to invoke flexoelectricity (and reliance only on incomplete metal screening as the mechanism behind intrinsic dead layer) cannot qualitatively reconcile the *ab initio* results (both ours as well as Ref. 15 calculations).

The outline of this paper is as follows. In Sec. II, after a brief summary of the pertinent concepts related to the flexoelectric phenomena, we solve the problem of a simple thin film based metal-insulator-metal capacitor system and highlight the relevance of flexoelectricity. The role of electric field penetration in metal electrodes is discussed in Sec. III and related to our central (flexoelectricity-based) results in Sec. II. We present the results of our model in Sec. IV with specific application to SRO/STO/SRO-based nanocapacitor system and draw a comparison with existing *ab initio* results of Stengel and Spaldin.[15] In this section, to elucidate the physical insights as well provide further prove of our conjectures, we also present *ab initio* calculations on other materials systems (Au/MgO/Au and Pt/MgO/Pt).

II. FLEXOELECTRICITY AND CONSEQUENCES FOR DEAD LAYER IN NANOCAPACITORS

In the traditional continuum field theory of piezoelectric materials, an electric polarization is generated in response to uniform strain (or vice versa). Within the assumptions of linearity, a third-rank piezoelectric tensor **d** relates the polarization vector **P** to the second-rank strain tensor **S**,

$$(P)_i = (d)_{ijk}(\mathbf{S})_{jk}. \tag{3}$$

With **d** being a third-order tensor, symmetry considerations require that it vanish for materials possessing a center of inversion symmetry. However, under conditions of nonuniform strain, the inversion symmetry in centrosymmetric materials can be broken to induce a net polarization. Phenomenologically, Eq. (3) can be extended to include the contribution of strain gradients

$$(P)_i = (d)_{ijk}(\mathbf{S})_{jk} + (\mu)_{ijkl}\nabla_l(\mathbf{S})_{jk}. \tag{4}$$

This added effect is referred to as the flexoelectric effect[19–22] and the components of the fourth order tensor μ are called the flexoelectric coefficients. The reader is referred to previous works for a review of this phenomena (e.g., Tagantsev,[21,23] and Cross[24]) and more recently our works.[25–27] Kogan[19] suggested that e/a is a suitable lower bound for the flexoelectric constants for crystalline dielectrics, where e is the electronic charge and a is lattice parameter. Others have suggested that multiplication by relative permittivity is more appropriate,[28] which now appears to have been confirmed experimentally.[17,18] Therefore high dielectric constant insulators such as nonpiezoelectric paraelectric STO are expected to exhibit large flexoelectric effects in certain directions. Furthermore, Fu *et al.*[29] experimentally reported an enhancement in the measured converse flexoelectric effect in BST samples due to the presence of electric field gradients. We note that Yang and co-workers[30,31] investigated the use of nonlocal polarization law to study the size effects and electromechanical coupling in thin-film nanocapacitors. Recently, Kalinin and Meunier[32] investigated flexoelectricity in low-dimensional nanostructures. Our recent atomistic simulations and calculations on prototype nanostructures[26] have revealed a striking enhancement in the effective piezoelectric constant of nearly 500% over bulk for tetragonal $BaTiO_3$ cantilever beam around 5 nm (and a corresponding 80% increase for the nonpiezoelectric cubic phase at the same size). In a more recent work,[27] we have also explored the use of the flexoelectric effect in nanostructures for energy harvesting applications. Results show a dramatic enhancement in energy harvesting for a narrow range of dimensions in such piezoelectric nanostructures. We have presented in previous works[26,33] a detailed mathematical theory of flexoelectricity. The governing equations valid for a dielectric occupying a volume V bounded by a surface S in a vacuum V' are

$$\nabla \cdot \sigma + \mathbf{f} = 0, \quad \text{where } \sigma = \mathbf{T} - \nabla \cdot \tilde{\mathbf{T}} \text{ in } V,$$

$$\bar{\mathbf{E}} + \nabla \cdot \tilde{\mathbf{E}} - \nabla \phi = 0 \text{ in } V,$$

$$-\varepsilon_0 \Delta\phi + \nabla \cdot \mathbf{P} = 0 \text{ in } V \text{ and } \Delta\phi = 0 \text{ in } V'. \tag{5}$$

σ may be considered as the actual physical stress experienced by a material point and differs from the Cauchy stress **T**. The remaining variables are defined through the following constitutive relations:

$$\mathbf{T} = \mathbf{c}:\mathbf{S} + \mathbf{e}:\nabla\mathbf{P} + \mathbf{d} \cdot \mathbf{P},$$

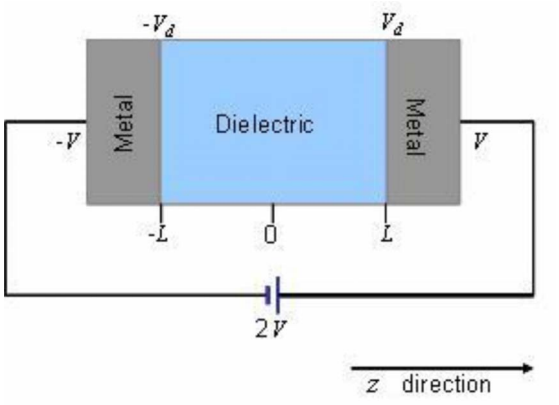

FIG. 1. (Color online) Schematic of a parallel-plate capacitor.

$$\tilde{\mathbf{T}} = \mathbf{f} \cdot \mathbf{P},$$

$$-\bar{\mathbf{E}} = \mathbf{a} \cdot \mathbf{P} + \mathbf{g}:\nabla\mathbf{P} + \mathbf{f}:\nabla\nabla\mathbf{u} + \mathbf{d}:\mathbf{S},$$

$$\tilde{\mathbf{E}} = \mathbf{b}:\nabla\mathbf{P} + \mathbf{e}:\mathbf{S} + \mathbf{g} \cdot \mathbf{P}. \tag{6}$$

The coefficients of the displacement, polarization, and their gradients defined above as "**a**," "**b**," "**c**," "**d**," "**f**," "**g**," and "**e**" are material property tensors. The second-order tensor **a** is the reciprocal dielectric susceptibility. The fourth order tensor **b** is the polarization gradient-polarization gradient coupling tensor, and **c** is the elastic tensor. The fourth order tensor **e** corresponds to polarization gradient and strain coupling introduced by Mindlin[22] whereas **f** is the fourth order flexoelectric tensor. **d** and **g** are the third order piezoelectric tensor and the polarization-polarization gradient coupling tensor. Further details may be obtained via consultation of Refs. 26 and 33.

The corresponding boundary conditions on S described by normal vector **n** are

$$\sigma \cdot \mathbf{n} = \mathbf{t}, \quad \text{where} \quad \sigma = \mathbf{T} - \nabla \cdot \tilde{\mathbf{T}},$$

$$\tilde{\mathbf{E}} \cdot \mathbf{n} = 0,$$

$$(-\varepsilon_0 \|\nabla\phi\| + \mathbf{P}) \cdot \mathbf{n} = 0. \tag{7}$$

The symbol $\| \|$ denotes the jump across the surface or an interface. We analyze the dielectric response of a thin-film capacitor system illustrated in Fig. 1. The dielectric is considered to have a cubic *centrosymmetric* lattice.[34] The one-dimensional flexoelectric equations (varying along the z direction) for the system shown in Fig. 1 reduce to

$$c_{11}\frac{\partial^2 u}{\partial z^2} + (e_{11} - f_{11})\frac{\partial^2 P}{\partial z^2} = 0,$$

$$(e_{11} - f_{11})\frac{\partial^2 u}{\partial z^2} + b_{11}\frac{\partial^2 P}{\partial z^2} - a_{11}P - \frac{\partial \phi}{\partial z} = 0,$$

$$-\varepsilon_0\frac{\partial^2 \phi}{\partial z^2} + \frac{\partial P}{\partial z} = 0. \tag{8}$$

The differential Eqs. (8) have to be solved subject to boundary conditions which we specify as follows. First, the mechanical force must vanish at the metal-dielectric interface which gives us our first boundary condition as

$$\left(c_{11}\frac{\partial u}{\partial z} + (e_{11} - f_{11})\frac{\partial P}{\partial z}\right)\Bigg|_{z=\pm L} = 0. \tag{9}$$

Also, due to the voltage drop in the metal due to electric field penetration, the actual potential $\pm V_d$ at the metal-dielectric interface will differ from the one applied $\pm V$ (see Fig. 1) and can be specified as

$$\phi|_{z=\pm L} = \pm V_d. \tag{10}$$

V_d remains to be determined.

While, the boundary conditions given by Eqs. (9) and (10) would be enough to solve the system in Fig. 1 in the absence of flexoelectricity (i.e., the case where $e_{11}=0$, $f_{11}=0$, and $b_{11}=0$), the presence of flexoelectricity requires the specification of an additional boundary condition, which may be taken as the specification of the polarization at the metal-dielectric interface by

$$P|_{z=\pm L} = -k\varepsilon_0 \eta V_d/L. \tag{11}$$

$\eta = \frac{\varepsilon_d - \varepsilon_0}{\varepsilon_0}$ is the dielectric susceptibility, where ε_d is the dielectric constant of the dielectric and k is a constant that controls the depth at which the electric field penetration occurs. The solution to the three independent fields displacement u, polarization P, and electric potential ϕ can be adapted from Mindlin[35] (who used a different physical theory, the so-called polarization gradient theory, but which has a mathematical structure similar to ours—our model contains his theory as well)

$$u = B_1 \cosh(z/l),$$

$$P = A_2 + B_2 \cosh(z/l),$$

$$\phi = A_3 z + B_3 \cosh(z/l). \tag{12}$$

Here,

$$B_3 = (1-k)\eta V_d/[\eta \sinh(L/l) + (L/l)\cosh(L/l)],$$

$$A_3 = (B_3/\eta l)\cosh(L/l) + kV_d/L,$$

$$A_2 = -\varepsilon_0 \eta A_3, \quad B_2 = \varepsilon_0 B_3/l = -c_{11}B_1/d_{11},$$

$$l = \{\varepsilon_0[b_{11}c_{11} - (e_{11} - f_{11})^2]/c_{11}(1 + \eta^{-1})\}^{-1/2}. \tag{13}$$

Note that the flexoelectric constants and e_{11} and f_{11} occur in the solution for the fields only through a length parameter l defined in Eq. (13). We will denote this length l as the longitudinal flexoelectric length scale. As claimed earlier, the solution to the governing equations of flexoelectricity confirm that strain gradients are automatically induced despite the absence of any external strain sources. The position de-

pendent "apparent" permittivity of the dielectric can be then written as

$$\varepsilon(z) = \frac{\varepsilon_0(1+\eta)A_3}{A_3 + (B_3/l)\cosh(z/l)}. \quad (14)$$

Finally, the capacitance of the dielectric layer C_d can be determined as the ratio between the electric displacement to the voltage across the layer as

$$C_d = \frac{(\varepsilon_0 \partial \phi - P)_{z=\pm L}}{2V_d} = \frac{\varepsilon_0(1+\eta)}{2L} \frac{1 + (k\eta l/L)\tanh(L/l)}{1 + (\eta l/L)\tanh(L/l)}. \quad (15)$$

As manifest from Eq. (15), for "large" thicknesses, the capacitance reverts to that predicted by classical electrostatics.

III. ELECTRIC FIELD PENETRATION

Now, we focus our attention on the remaining constituent of the capacitor, i.e., the metal electrode. In the conventional picture of a capacitor, the electrode is an ideal metal and the electrical field inside the dielectric is perfectly screened. However, both experiments and *ab initio* simulations have shown that in real systems, screening of electric fields takes place over a finite spatial extent inside the metal. Because of the penetration of electric field into the metal, there is a potential drop inside the metal electrode which then introduces an additional capacitance into the system [apart from that due to the dielectric Eq. (15)]. Typically, this effect is modeled by requiring the free charges in the electrode to form a layer of finite thickness at the metal-dielectric interface. In the conventional picture of a capacitor, the free charges reside at an infinitesimally thin layer at the metal-dielectric interface as a delta function and there is no separation between them and the polarization bound charge in the dielectric. However, when a free charge layer of finite thickness is assumed in the electrode, the center of charge in the electrode is separated by a finite distance from the polarization bound charge in the dielectric and an additional capacitance is introduced. Also, as one can infer from the electrostatic Poisson's equation, a finite spatial distribution of charges inside the electrode results in electric fields penetrating into the metal electrode: a scenario which is forbidden in the conventional description of a capacitor. Dawber and Scott[12] provided a description of the phenomenon of electric field penetration into metal electrodes based on the Drude model for a free-electron gas in contact with a dielectric and arrived at physically insightful analytical expressions for the charge-density distribution $\rho(z)$ and the electric field $E(z)$ inside the electrodes

$$\rho(z) = \frac{Q}{\lambda}\exp\left(\frac{-|z|+L}{\lambda}\right), \quad E(z) = -\frac{Q}{\varepsilon_e}\exp\left(\frac{-|z|+L}{\lambda}\right). \quad (16)$$

λ is the Thomas-Fermi screening length and is related to the static conductivity σ_0, diffusion coefficient D, and the dielectric constant of the metal electrode ε_e as $\lambda = (\frac{4\pi\sigma_0}{D\varepsilon_e})^{-1/2}$. From the potential distribution, the corresponding capacitance of the metal electrode C_e is $\frac{\varepsilon_e}{\lambda}$. Since the potential drop is supposed to happen entirely in an electron-gas-like medium, the dielectric constant ε_e is typically taken as that of free space. For an SRO electrode in the system under consideration, with $\lambda = 0.5$ Å,[12] the value of this capacitance is $\sim 177\text{fF}\ \mu\text{m}^{-2}$; the net contribution to the capacitance due to both the electrodes is therefore around $88\text{fF}\ \mu\text{m}^{-2}$. Hence, the capacitance of the whole system (after including the contribution due to the dielectric layer) cannot be larger than $88\text{fF}\ \mu\text{m}^{-2}$. However, the capacitance of the SRO/STO/SRO system as found by Stengel and Spaldin[15] is $\sim 258\text{fF}\ \mu\text{m}^{-2}$. Clearly, this approach overestimates the capacitance contribution due to the metal electrodes. A major criticism to this approach is that the capacitance contribution to metal electrode is independent of the size and the material properties of the dielectric region. It should also be noted that yet another approach to model the electric field penetration into metal electrodes involves consideration of the band structure of metal/dielectric interface.[36] However, the capacitance contributions of the metal electrodes using this approach are again overestimated. In order to address this issue, we propose an alternate approach to model the penetration of electric fields into the metal electrodes. The idea of an abrupt metal/dielectric interface, especially while modeling phenomena varying at the level of a few angstroms, is questionable since one would expect the atoms at the interface to have bonding that is intermediate in nature to that in the metal electrode and the dielectric. In order to model the diffuse interface, we will let the dielectric permittivity at the interface to be a continuously varying function of position.[37] Though the interface extends both into the metal and the dielectric, we will only subject the dielectric permittivity of the metal to the variation. In order to do so, we choose that the inverse dielectric permittivity of the metal $1/\varepsilon_e(z)$ has the following functional form:

$$\frac{1}{\varepsilon_e(z)} = A\exp\left(-\frac{|z+L|}{l_v}\right). \quad (17)$$

The constant A is the inverse permittivity of the dielectric at the metal/dielectric interface which can be obtained by substituting $z=L$ in Eq. (14) and l_v is the length scale associated with the variation: the smaller the parameter l_v, the sharper is the variation in the dielectric constant in the metal. Equations (14) and (17) provide the dielectric permittivity profiles in the dielectric and the metal, respectively.

IV. THEORETICAL RESULTS, FIRST-PRINCIPLES CALCULATIONS, AND PHYSICAL INSIGHTS

In this section we apply the preceding analysis to a SRO/STO/SRO capacitor system which has been investigated using *ab initio* methods by Stengel and Spaldin.[15] The dimensions of the capacitor ($2L=2.7$ nm), voltage applied ($2V=27.8$ mV), and the bulk permittivity of the dielectric STO (~ 490) are the same as the ones used in Ref. 15. The flexoelectric coefficients for STO have been determined by employing the approach of Askar and co-workers[38,39] and the longitudinal flexoelectric length scale is found to be 1.51 Å.

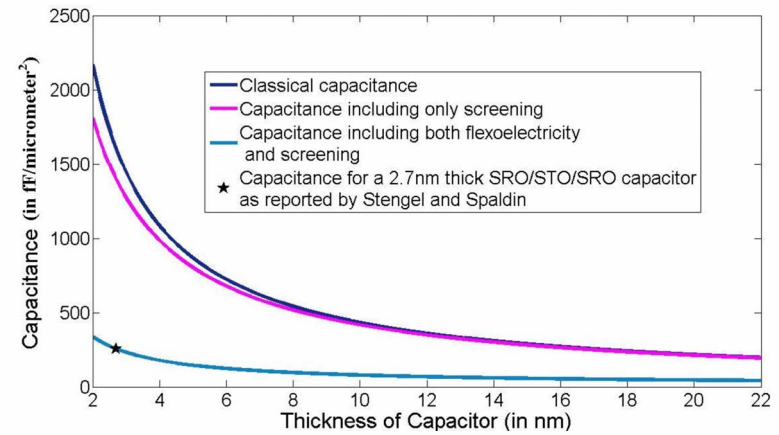

FIG. 2. (Color online) Thickness-size-dependent capacitance of SRO/STO/SRO capacitor. Only if both electric field penetration and flexoelectricity are considered, we get a good agreement with *ab initio* calculations.

However it is found that the transverse flexoelectric length scale is as large as ~3 nm. The relatively large transverse value is the reason behind observation of large flexoelectricity effects only in shearing or bending experiments[17,18] but does not enter the one-dimensional equations for our particular problem. Yet approximately, the method is giving a reasonable estimate. In a more recent work, we have used a more rigorous method[40] following Tagantsev's approach and found a good agreement with the experimental values of Zubko *et al.*[18] The constant k is estimated from the average dielectric permittivity of the system in the *ab initio* calculations of Ref. 15 as 0.3 and the transition length scale is 2.0 Å. With these parameters and use of Eq. (15), we are able to find a good quantitative agreement with the *ab initio* results of Ref. 15: 256fF μm^{-2}. The major insights however lie in the qualitative comparison and the scaling of capacitance which we now proceed to make.

In Fig. 2, we plot the scaling of capacitance with size as predicted by (i) classical electrostatics, (ii) if only the flexoelectricity mechanism is operative, (iii) if only electric field penetration is operative, and finally (iv) if both flexoelectricity and electric field penetration are operative. The lone data point available from *ab initio* calculations of Ref. 15 is also shown. Results clearly illustrate that neither flexoelectricity alone nor electric field penetration alone can reconcile the *ab initio* results correctly and both are (not only present) but needed. To further appreciate the latter statement, we note that if only electric field penetration is considered as the mechanism, the scaling of capacitance with size cannot be reconciled. Flexoelectricity however is insufficient (by itself) to quantitatively match the *ab initio* results.

The voltage at the metal/dielectric interface 6.80 mV and the electric field in the middle of the dielectric (1.6 V μm^{-1}) compare favorably to the *ab initio* results. The profile of electrostatic potential (Fig. 3) also exhibits a reasonable match. We note that the degree of nonlinearity of the induced potential predicted by the continuum flexoelectric theory (as opposed to the linear behavior predicted by classical electrostatics) depends crucially upon the size of the thin film and the bulk dielectric permittivity of the constituent insulating material. For a bulk-sized film, the nonlinearity in the potential profile predicted by flexoelectricity confines itself to a very small region near the interface: the resulting change in capacitance is therefore negligible and hence this effect is of little or no consequence for such bulk-sized films. Further, this nonlinearity also depends directly upon the dielectric permittivity of the material: i.e., the better the dielectric, the larger is the nonlinearity in the induced potential and the consequent adverse impact on the capacitance. Therefore it is expected that nanometer-sized thin-film capacitors made of high-permittivity materials such as ferroelectric perovskites will be the most affected by the adverse impact of flexoelectricity. Indeed *ab initio* simulations on nanometer-sized Pt/MgO/Pt systems[15] (dielectric constant ε of MgO is 9.8) show virtually no anomalous capacitance behavior. In the remaining of this work, we try to investigate further the relevance of this conclusion using first-principles calculations on Au/MgO/Au and Pt/MgO/Pt nanocapacitors. We also point out the challenges beyond such calculations.

Most of the finite electric field calculations within the framework of density functional theory (DFT) are based on the Berry phase formalism. However, in the case of realistic nanocapacitors with a metal-dielectric interface, the requirement of a unique Fermi level in DFT calculations is broken. In the presence of electric field, an effective bias potential is induced due to the shift in the Fermi levels creating a par-

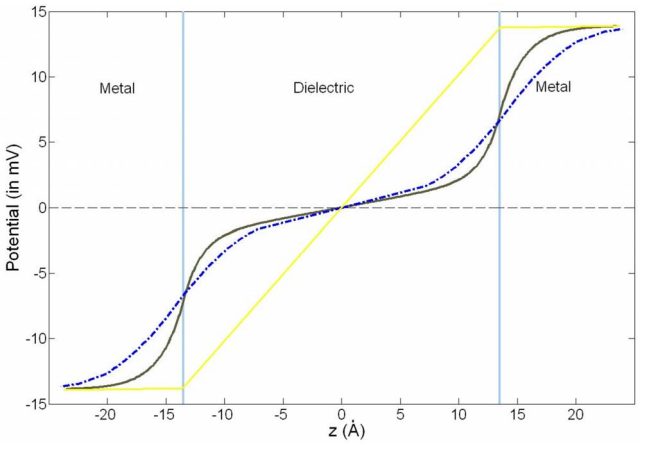

FIG. 3. (Color online) Comparison of the potential profile inside the SRO/STO/SRO capacitor system obtained by continuum flexoelectricity (dash dot blue curve) with that obtained by Stengel and Spaldin (Ref. 15) using *ab initio* techniques (solid black curve). Yellow (light gray) curve is the potential expected from classical electrostatics.

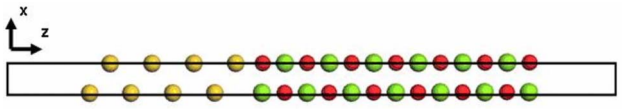

FIG. 4. (Color online) Au/MgO simulated supercell. The metal (Au in yellow) is put into contact with the magnesium oxide (Mg in green and O in red) inside vacuum (right and left empty space).

tially occupied states at the energy gap of the dielectric.[41] A possible method to overcome this difficulty with finite electric field is provided by the nonequilibrium Green's functions, but this method turns out to be not computationally efficient. Stengel and Spaldin[15,41] implemented an alternative method based on Wannier-function theory to correctly simulate the metal/insulator/metal (MIM) system. They also suggested another approach, which uses conventional *ab initio* codes such as Vienna *ab initio* simulation package (VASP) and (plane wave self-consistent field (PWSCF), by simulating only the metal/insulator (MI) in the presence of vacuum. This method was successfully implemented by Lee *et al.*[42] and used to calculate the capacitance of Au/MgO/Au and $Ni/ZrO_2/Ni$ systems.

We used VASP (Ref. 43) to study a system of Au/MgO(100)/Ag and Pt/MgO(100)/Pt. Only the metal/insulator slab (half of the realistic capacitor is modeled) with both sides exposed to vacuum in the presence of external electric field (to model the voltage bias between the electrodes) is simulated (see Fig. 4). A uniform electric field is applied along the z direction and is modeled by adding a sawtooth-like potential to the external potential entering the Kohn-Sham equations. We used the projector augmented wave (PAW) (Ref. 44) potentials to describe the ionic potentials and local density approximation to represent the exchange-correlation energies. A regular $6\times6\times1$ k-points mesh and 400 eV energy cutoff were employed. A Gaussian smearing with width 0.5 eV was used to describe the partial occupancies for each wave function. The longitudinal lattice mismatch between gold and the oxide is within 1% whereas the transversal lattice constants considered are those of the oxide (in-plane lattice parameters were set to 4.15 nm). The system is then relaxed until Hellmann-Feynman forces on each atom are below 0.02 eV/A. Since the system under study has nonpolar-terminated surfaces, we do not need to treat or passivate the surfaces. The vacuum region in each supercell was large enough to avoid wave-function overlaps and interactions between neighboring supercells. The plane-wave basis set used in most of the DFT calculations assumes a full periodicity of the supercell geometry and the electrostatic potential. In general, for surface supercell calculations in vacuum, the simulated slabs can be asymmetric which means that the periodic boundary condition is not satisfied since the electrostatic potential value will be different on the boundary of each neighboring supercells. Bengtsson[45] provided a solution to the potential mismatch at the boundary by introducing an artificial dipole correction to the energy expression for periodic supercell calculations. Such correction was implemented in VASP package and used to correctly estimate the electrostatic potential for supercell slab calculations in vacuum. A restriction to this technique is that the internal

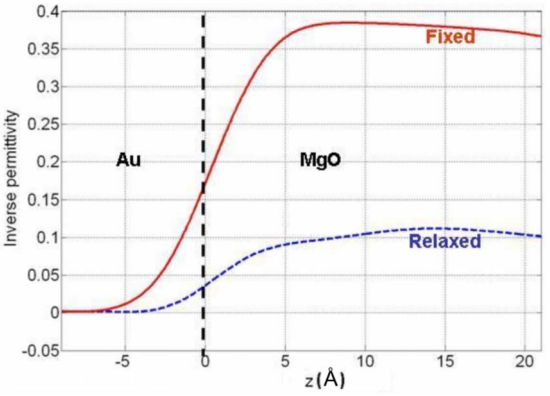

FIG. 5. (Color online) Au/MgO inverse local permittivity profile. Blue dashed line and solid red line are, respectively, for the relaxed and fixed ions simulations.

electric filed is limited by the permittivity of the dielectric. The internal electric field is equal to the external electric field in the vacuum divided by the dielectric constant. Hence, for high-permittivity dielectric such as $SrTiO_3$, only small values of the electric fields are allowed. One more limitation is that the terminated surface of the insulator needs to be nonmetallic otherwise we will recover the same situation in MIM system.

In order to obtain the total local potential and permittivity profiles, an averaging technique is used to smooth the variations. We consider a 0.1 eV/Å external electric field E_{ext} applied along the axial z direction of the MI system. The ions are relaxed in response to the applied electric filed.

The change in electrostatic potential ΔV is defined as the difference in electrostatic potentials V in the presence and in the absence of external electric field (averaged over the in-plane xy cross section)

$$\Delta V(z) = \frac{1}{ab}\int_0^a \int_0^b [V(x,y,z)|_{E_{\text{ext}}} - V(x,y,z)|_{E_{\text{ext}}=0}]dydx\,. \tag{18}$$

The constants a and b, respectively, designate the unit-cell lengths along the x and y directions.

To soften the variation of ΔV, we take a macroscopic average over the bulk periodicity l_1 and l_2, respectively, of the metal and insulator as defined by Ref. 46

$$\langle \Delta V(z)\rangle = \frac{1}{l_1 l_2}\int_{z-l_1/2}^{z+l_1/2}\int_{z'-l_2/2}^{z'+l_2/2}\Delta V(z'')dz''dz'\,. \tag{19}$$

Hence, the local permittivity is simply expressed in terms of the external electric field and the local potential

$$\langle \varepsilon(z)\rangle = -\frac{E_{\text{ext}}}{\frac{d}{dz}\langle \Delta V(z)\rangle}\,. \tag{20}$$

Figure 5 represents the variation of the local dielectric constant inside the metal Au and insulator MgO for both fixed and relaxed calculations. The static permittivity (Fig. 5: dashed blue curve) can be decomposed into ionic and elec-

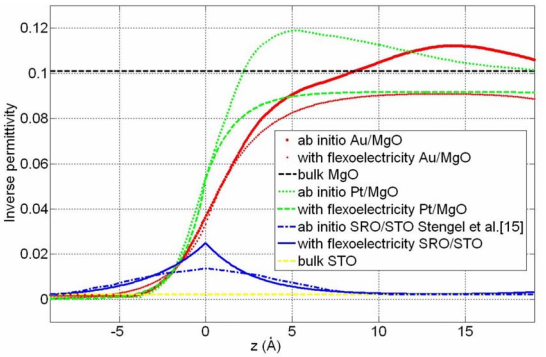

FIG. 6. (Color online) Inverse dielectric permittivity profiles for Au/MgO, Pt/MgO and SRO/STO. The horizontal dashed black (dark dashed gray) and yellow lines (light dashed gray) are, respectively, the bulk MgO and STO inverse static permittivity. Results show a good agreement and match the bulk limit in the middle of the dielectric.

tronic contributions and is evaluated by letting the ions to relax freely under applied bias. The electronic response corresponds to the so-called optical permittivity (Fig. 5: solid red curve) that can be obtained by fixing the ions to their zero electric field equilibrium configurations.

Ideally, the dielectric constant in metals is infinite, but near the electrode-insulator interface there is an electric field penetration. This exactly corresponds to a zero inverse permittivity in the metal that increases as one approach closer to the metal-insulator interface—in good agreement with the simulated profile. The static and optical dielectric constants are estimated to be 9.52 and 2.78, compared to 9.65 and 3.36 of Ref. 42.

A comparison between our theoretical model (incorporating flexoelectricity and electric field penetration effects) and the *ab initio* calculation of the inverse permittivity profile is illustrated in Fig. 6. Results show a good agreement between the theory and first-principles simulations. Curves tend to the bulk inverse static permittivity in the middle of the insulator. Our SRO/STO/SRO theoretical results match the *ab initio* simulations carried out by Stengel and Spaldin[15] for these nanocapacitor systems. Moreover, our Au/MgO/Au and Pt/MgO(100)/Pt calculations show a good agreement and capture the right profile of the static permittivity with no anomalous behavior at the interface as expected for such low-permittivity materials.

V. CONCLUSION

Toward a better understanding of the phenomena beyond the dead layer at the electrode-dielectric interface, we have provided a theoretical model incorporating flexoelectricity combined with an approach to electric field penetration inside metals that is able to explain well the first-principles calculations performed by Stengel and Spaldin[15] and our own calculations carried out on Au/MgO/Au and Pt/MgO(100)/Pt nanocapacitors. Results indicate that both flexoelectricity and electric field penetration inside metal are essential to reconcile the atomistic simulations. Hence, flexoelectricity has an important contribution which opens the possibility of providing a remedy to the dead layer in nanocapacitors by carefully designing the metal-dielectric interface. Such an endeavor, based on the present results, will be taken in the future. It is also relevant to mention that some experimental works (e.g., Saad *et al.*[47]) on single-crystal barium titanate nanocapacitors reported an absence of size effects and a dielectric response comparable to large crystals in contrast with conventional thin-film nanocapacitors. It would be interesting to study such systems in future work.

ACKNOWLEDGMENTS

Financial support from NSF NIRT Grant No. CMMI 0708096 is gratefully acknowledged.

*Corresponding author: psharma@uh.edu

[1] C. Zhou and D. M. Newns, J. Appl. Phys. **82**, 3081 (1997).
[2] C. A. Mead, Phys. Rev. Lett. **6**, 545 (1961); Phys. Rev. **128**, 2088 (1962).
[3] M. McColl and C. A. Mead, Trans. Metall. Soc. AIME **233**, 502 (1965).
[4] C. Basceri, S. K. Streiffer, A. I. Kingon, and R. Waser, J. Appl. Phys. **82**, 2497 (1997).
[5] S. K. Streiffer, C. Basceri, C. B. Parker, S. E. Lash, and A. Kingon, J. Appl. Phys. **86**, 4565 (1999).
[6] N. Yanase, K. Abe, N. Fukushima, and T. Kawakubo, Jpn. J. Appl. Phys., Part 1 **38**, 5305 (1999).
[7] D. J. Kim, J. Y. Jo, Y. S. Kim, Y. J. Chang, J. S. Lee, J. G. Yoon, T. K. Song, and T. W. Noh, Phys. Rev. Lett. **95**, 237602 (2005).
[8] R. Kretschmer and K. Binder, Phys. Rev. B **20**, 1065 (1979).
[9] S. P. Alpay, I. B. Misirlioglu, V. Nagarajan, and R. Ramesh, Appl. Phys. Lett. **85**, 2044 (2004).
[10] M. W. Chu, I. Szafraniak, R. Scholz, C. Harnagea, D. Hesse, M. Alexe, and U. Gosele, Nature Mater. **3**, 87 (2004).
[11] C. T. Black and J. J. Wesler, IEEE Trans. Electron Devices **46**, 776 (1999).
[12] M. Dawber and J. F. Scott, Jpn. J. Appl. Phys., Part 1 **41**, 6848 (2002).
[13] A. K. Tagantsev and G. Gerra, J. Appl. Phys. **100**, 051607 (2006).
[14] N. A. Pertsev, R. Dittman, R. Plonka, and R. Waser, J. Appl. Phys. **101**, 074102 (2007).
[15] M. Stengel and N. A. Spaldin, Nature (London) **443**, 679 (2006).
[16] G. Catalan, L. J. Sinnamon, and J. M. Gregg, J. Phys.: Condens. Matter **16**, 2253 (2004).
[17] W. Ma and L. E. Cross, Appl. Phys. Lett. **78**, 2920 (2001); **79**, 4420 (2001); **81**, 3440 (2002); **82**, 3293 (2003).
[18] P. Zubko, G. Catalan, P. R. L. Welche, A. Buckley, and J. F. Scott, Phys. Rev. Lett. **99**, 167601 (2007).
[19] S. M. Kogan, Fiz. Tverd. Tela (Leningrad) **5**, 2829 (1963).
[20] V. L. Indenbom, V. B. Loginov, and M. A. Osipov, Kristal-

lografiya **28**, 1157 (1981).
[21] A. K. Tagantsev, Phys. Rev. B **34**, 5883 (1986).
[22] R. D. Mindlin, Int. J. Solids Struct. **4**, 637 (1968).
[23] A. K. Tagantsev, Phase Transitions **35**, 119 (1991).
[24] L. E. Cross, J. Mater. Sci. **41**, 53 (2006).
[25] A. K. Taganstev, V. Meunier, and P. Sharma, MRS Bull. (to be published).
[26] M. S. Majdoub, P. Sharma, and T. Cagin, Phys. Rev. B **77**, 125424 (2008); arXiv:0903.0785, Phys. Rev. B (to be published).
[27] M. S. Majdoub, P. Sharma, T. Cagin, Phys. Rev. B **78**, 121407(R) (2008).
[28] M. Marvan and A. Havranek, Solid State Commun. **101**, 493 (1997).
[29] J. Y. Fu, W. Zhu, N. Li, and L. E. Cross, J. Appl. Phys. **100**, 024112 (2006).
[30] J. S. Yang, Int. J. Appl. Electromagn. Mech. **8**, 307 (1997).
[31] J. S. Yang, Scott X. Mao, K. Yan, and A.-K. Soh, Scr. Mater. **54**, 1281 (2006).
[32] S. V. Kalinin and V. Meunier, Phys. Rev. B **77**, 033403 (2008).
[33] R. Maranganti, N. D. Sharma, and P. Sharma, Phys. Rev. B **74**, 014110 (2006).
[34] The *ab initio* calculations in Ref. 15 are for centrosymmetric system and such an assumption is adopted to allow a comparison of results.
[35] R. D. Mindlin, Department of Civil and Engineering Mechanics, University of Columbia–New York Report. No. 4, 1969 (unpublished).
[36] H. Y. Ku and F. G. Ullman, J. Appl. Phys. **35**, 265 (1964).
[37] F. Stern, Phys. Rev. B **17**, 5009 (1978).
[38] A. Askar, P. C. Y. Lee, and A. S. Cakmak, Phys. Rev. B **1**, 3525 (1970).
[39] A. Askar, and P. C. Y. Lee, Phys. Rev. B **9**, 5291 (1974).
[40] R. Maranganti, and P. Sharma, arXiv:0903.0684 (unpublished).
[41] M. Stengel and N. A. Spaldin, Phys. Rev. B **75**, 205121 (2007).
[42] B. Lee, C. Lee, S. Han, J. Lee, and C. S. Hwang, J. Appl. Phys. **103**, 024106 (2008).
[43] G. Kresse and J. Hafner, Phys. Rev. B **47**, 558 (1993).
[44] P. E. Blöchl, Phys. Rev. B **50**, 17953 (1994).
[45] L. Bengtsson, Phys. Rev. B **59**, 12301 (1999).
[46] A. Balderschi, S. Baroni, and R. Resta, Phys. Rev. Lett. **61**, 734 (1988).
[47] M. M. Saad, P. Baxter, R. M. Bowman, J. M. Gregg, F. D. Morrison, and J. F. Scott, J. Phys.: Condens. Matter **16**, L451 (2004).